



Coupled magnetic nanoparticle-mediated isolation and single-cell image recognition to detect *Bacillus* cell size in soil

Nan Rong^{1,2} | Shiying He^{3,4} | Bei Li^{5,6} | Xiangui Lin¹ | Xiaoling Liu⁷ |
Yongjie Yu^{1,8}  | Youzhi Feng¹ 

¹State Key Laboratory of Soil and Sustainable Agriculture, Institute of Soil Science, Chinese Academy of Sciences, Nanjing, China

²School of Resources and Environment, University of Chinese Academy of Sciences, Beijing, China

³Institute of Agricultural Resources and Environment, Jiangsu Academy of Agricultural Sciences, Nanjing, China

⁴School of environmental and safety engineering, Jiangsu University, Zhenjiang, China

⁵Changchun Institute of Optics, Fine Mechanics and Physics, Chinese Academy of Sciences, Changchun, China

⁶HOOKE Instruments Ltd, Changchun, China

⁷State Key Laboratory of Environmental Criteria and Risk Assessment, Chinese Research Academy of Environmental Sciences, China

⁸MNR & Guangxi Key Laboratory of Karst Dynamics, Institute of Karst Geology, Chinese Academy of Geological Sciences, Guilin, China

Correspondence

Yongjie Yu and Youzhi Feng, State Key Laboratory of Soil and Sustainable Agriculture, Institute of Soil Science, Chinese Academy of Sciences, Nanjing, 210008, China.

Email: yjyu@nuist.edu.cn and yzfeng@issas.ac.cn

Funding information

Guangxi Key Science and Technology Innovation Base on Karst Dynamics, Grant/Award Number: 202008; National Natural Science Foundation of China, Grant/Award Numbers: 41771294, 42177297; the Natural Science Foundation of Beijing, China, Grant/Award Number: 8182058

Abstract

Microbial morphology fundamentally constrains how species interact with their environment, and hence ultimately affects their niche. However, the methodology of functional microbes in the soil ecosystem is still poorly studied since it is difficult to capture and identify the active monospecific community from the complicated environment and enormous number of microbial species in soils. To comprehensively reveal the morphology of active microbes in soil ecosystem, magnetic nanoparticle-mediated isolation (MMI) and single-cell image recognition (SCIR) were employed to study soil active *Bacillus* community, which functionally boosted the soil fertility in organic fertilisation compared to mineral fertilisation and unfertilised control treatments in our previous study. The results showed that MMI and SCIR can efficiently isolate active *Bacillus* from soil particles and other microorganisms. High throughput sequencing showed that the captured *Bacillus* showed similar community structure in different long-term fertilisation soils, while SCIR revealed that the active *Bacillus* was greater in number and larger in size in organic fertilisation treatment compared to mineral fertilisation and unfertilised control treatments. Our study demonstrates that the combination of MMI and SCIR is a potentially powerful tool to capture and identify the morphology of active and functional microbes in the soil ecosystem.

KEYWORDS

Bacillus, cell size, fertilisation, magnetic nanoparticle-mediated isolation, single-cell image recognition

1 | INTRODUCTION

One of the most important classic and contemporary interests in microbial ecology is the connection between active functional microorganisms and habitat. Cell size is a key determinant of microbial function, and cell function also affects cell size (Portillo et al., 2013). Thus, cell size fundamentally constrains how species interact with their environment (Healy et al., 2013). For example, cell diameter is inversely related to the surface-to-volume ratio of cells, which is associated with the rate of growth, cell division, and the absorption of nutrients (Portillo et al., 2013; Young, 2006). To a large extent, the diversity of function in the cell is the result of diversity in size (Miettinen & Bjorklund, 2016; Miettinen & Bjorklund, 2017). The current understanding is that cell size is affected by both the internal factors and the external environment (e.g., nutrients) (Ginzberg et al., 2015; Lloyd, 2013), which further influence cellular metabolic activity (Bjorklund, 1866). Under an ideal environment, microorganisms tend to grow exponentially with little variation in body size (Chien et al., 2012). In contrast, microbial body size varies greatly when microorganisms are exposed to environmental pressures (Hill et al., 2012). In this respect, microbial morphology could act as a proxy reflecting environmental conditions. Combining microbial morphology with microbial community information can help to unravel the comprehensive responses of microorganisms to an external perturbation.

Most of the existing microbial morphology studies focused on purified strains (Chen et al., 2020; Ursell et al., 2017). Understanding the microbial morphology of active functional bacteria in soils is still a great challenge due to the dispersal of microorganisms within a high load of (background) soil particles (Eichorst et al., 2015). To solve this problem, microbiologists almost always set focus on two key points: one is how to isolate target microorganisms from complex soil samples, and the other is how to observe the morphological characteristics of the isolated microorganisms. Almost all technologies are unable to recover live, functional bacteria from soil samples, except magnetic nanoparticle (MNP)-mediated isolation (MMI) (Zhang et al., 2015). The principle of the MMI method is to magnetise all the microbial cells of the whole sample with MNPs. Only the microorganisms with metabolic activity will decrease their surface MNPs due to continuous cell division and proliferation until they lose magnetism. Finally, by separating dividing bacteria from non-dividing (i.e., non-metabolically active) bacteria and soil particles by maintaining magnetism via an external magnet (Li et al., 2018; Wang et al., 2016; Zhang et al., 2015), Zhang et al. successfully isolated a group of previously uncultured phenol degraders, *Burkholderiales*

sp., from a sewage treatment system using the MMI method (Zhang et al., 2015). Furthermore, single-cell image recognition (SCIR) was developed as a prospective technology to investigate the morphology of the active microbes isolated by MMI. Gan et al. (2021) successfully identified and located active iron-reducing microorganisms from both pure culture and sediment-containing samples by coupling fluorescent and chemosensor confocal laser scanning microscopy at the single-cell level. However, coupling MMI and SCIR for visualisation of active functional microorganisms and evaluation of their size even at the single-cell level is still lacking in studies of the soil ecosystem.

About 30% of arable land in the world suffers from alkaline conditions that limit crop production (Takahashi et al., 2001), and this challenge is compounded by increasing aridity at the global scale (Berdugo et al., 2020; Slessarev et al., 2016). Wheat and maize are among the most widely grown commodity crops in the world, accounting for a considerable amount of cropland arable area, yielding non-meat calories and animal feed (Lobell & Field, 2007). It has been demonstrated that *Bacillus* could be a functional bacterial species in promoting soil fertility and crop yield via accelerating carbon and phosphorus cycling in alkaline soils (Feng et al., 2015). Unlike most bacteria that generally cannot decompose macromolecules, *Bacillus* can naturally secrete a wide range of hydrolytic enzymes that can decompose complex organic matter and release mineral nutrients (such as phosphonate) into their environment (Pohl & Harwood, 2010), making them the keystone taxa in enhancing soil fertility. Hence, the insight into the response of *Bacillus* to distinct fertilisation strategies could provide critical information for dryland ecosystems that suffer from alkaline soils on a global scale. *Bacillus* is able to resist extreme environments by forming endospores (Nicholson et al., 2000), so the *Bacillus* cell can still grow and divide even after inactivation by hyperthermia. The magnetism of *Bacillus* is gradually lost, while that of the non-dividing cells and soil particles remains; therefore, they can be separated by external magnets. So far, rare studies have isolated active *Bacillus* from soil environment using MMI, much less identified the morphology by SCIR.

In this study, we applied MMI and SCIR methods in three typical fertilised soils from a 30-year long-term fertilisation field experiment in the Northern China Plain, where winter wheat-summer maize rotation is the dominant cropping system, and crop production is largely constrained by the lower indigenous fertility of the alkaline soil (Feng et al., 2015). Since a *Bacillus* species, *B. asahii*, was found to be important in improving soil fertility and supporting higher crop yield at this sampling site,

we hypothesize that organic fertilisation might cultivate a *Bacillus* community with a larger cell size compared to unfertilized control. To address this issue, MMI combined with SCIR was employed to investigate the cell size of metabolically active *Bacillus*, isolated from soils in a long-term field experiment encompassing three fertilisation regimes: mineral fertilisation (MF), organic fertilisation (OF), and unfertilized control (CK).

2 | MATERIALS AND METHODS

2.1 | Site description and sample collection

Soil samples were collected from a long-term fertilisation experiment field located at Fengqiu Agroecological Experimental Station (35°00'N, 114°24'E) in Henan Province, China. The mean annual temperature is 13.9°C and the mean annual precipitation is 615.1 mm. The soil, characterised by a sandy loam texture, contained 5.8 g kg⁻¹ organic C, 0.56 g kg⁻¹ total N, 0.88 g kg⁻¹ total phosphorus (P₂O₅), 29.3 g kg⁻¹ total potassium (K₂O), and pH (1:2.5 v/w) of 8.5 at the onset of the experiment in 2011. The plot experiment was conducted under a rotation of winter wheat (*Triticum aestivum* L.) and summer maize (*Zea mays* L.). The treatments included mineral fertilisers (MF), organic fertilisers (OF), and unfertilized control (CK). Four replicated plots of 30 m² were established randomly for each fertiliser treatment. For the MF treatment, N, P, and K were applied in the form of urea (200 kg N ha⁻¹), superphosphate (80 kg P₂O₅ ha⁻¹), and potassium sulphate (150 kg K₂O ha⁻¹), respectively. The MF and OF treatments were designed to supply the same amount of total N. In the OF treatment, one-half of N came from urea and the other half was from mushroom residues. All P, K, and organic residues were applied as basal fertilisers, whereas urea was applied to the two fertilisation treatments as both basal and supplementary fertilisers. Basal fertilisers were evenly broadcast onto the soil surface and were incorporated into the ploughed layer before sowing in June for maize and in October for wheat. Supplementary fertiliser urea was surface applied by hand and then brought into the ploughed layer when irrigating.

Soil samples were collected in August 2019. For each plot, 20 cores of topsoil (0–20 cm) were sampled using a 30-mm-diameter gouge auger following the serpentine sampling method. The soils for each plot were blended as a composite representative for that plot and then sieved (<2 mm) to remove particles and plant roots. Part of each composite was air-dried for chemical analysis, and the remaining was stored at 4°C for further experiment.

TABLE 1 Soil chemical properties of three fertilisation treatments

Treatment	pH	SOC g kg ⁻¹	Total N g kg ⁻¹	Available N mg kg ⁻¹	Total P g/kg	Available P mg kg ⁻¹	Total K g kg ⁻¹	Available K mg kg ⁻¹
CK	8.41 a ± 0.04	5.19 b ± 0.07	0.54 b ± 0.02	57.24 c ± 2.47	1.16 c ± 0.08	1.95 b ± 0.28	9.53 b ± 0.32	49.6 c ± 5.27
MF	8.25 b ± 0.07	5.8 b ± 0.13	0.63 b ± 0.02	68.08 b ± 2.64	1.73 b ± 0.21	6.81 b ± 2.30	11.8 a ± 0.73	111.25 b ± 8.66
OF	8.21 b ± 0.06	11.50 a ± 0.74	1.09 a ± 0.07	106.16 a ± 6.05	2.13 a ± 0.09	47.55 a ± 13.92	11.53 a ± 0.43	163.25 a ± 23.67

Abbreviations: CK, unfertilised control; K, potassium; MF, mineral fertilisation; N, nitrogen; OF, organic fertilisation; P, phosphorus; SOC, soil organic carbon.

Details of soil chemical properties of three fertilisation regimes are listed in Table 1.

2.2 | MNPs-mediated *Bacillus* isolation and cell size measurement

The specific experimental process includes three parts: (1) determination of the optimal ratio of soil suspensions and MNPs; (2) isolation of *Bacillus* from the soil sample by enrichment and cultivation; (3) image acquisition of *Bacillus*.

Briefly, MNP was synthesised using the co-precipitation method (Lu et al., 2007). Magnetic nanoparticles (MNPs) were stabilised for 10 min in an ultrasound bath at 40 kHz before being used. Two soil suspensions in water (1:10 mass/volume ratio) were prepared for each treatment, and the large-grain soil and impurities therein were removed by centrifugation at $1000 \text{ r} \cdot \text{min}^{-1}$ for 2 min. To test the soil magnetic functionalization efficiency for effective separation, 10 ml soil suspensions for each treatment were mixed with different weights (from 0.4 to 2.4 g at a step of 0.4 g) of synthesised MNPs. After shaking (150 rpm) for 20 min, the magnetic functionalized soils were harvested using a permanent magnet for 10 min, and the remaining supernatant was also collected. Quantitative polymerase chain reaction (qPCR) was used to quantify the bacterial concentration in the supernatant (bacterial 16S rRNA copy numbers in magnetic-free fraction, termed BCMF hereafter, copies/mL) and soil pellet wrapped by MNPs (termed BCMS hereafter, copies/mL), respectively. The soil magnetic functionalization efficiency was calculated using the expression: $E = \text{BCMS}/[\text{BCMF} + \text{BCMS}]$ (Wang et al., 2016). Here, an optimal ratio was determined when soil magnetic functionalization efficiency reached 100%, namely the inflection point, where bacteria in the soil suspension were just wrapped by MNPs. A soil magnetization efficiency of over 100% indicated excess MNPs over the initial bacteria would continue to encapsulate the newly reproduced bacteria going forward. On the contrary, when the soil magnetization efficiency is less than 100%, the MNPs content is too low to enwrap all the bacteria, resulting in the loss of some target microorganisms.

The enrichment medium of *Bacillus* was prepared as the following formula: peptone 10 g/L, yeast extract 3 g/L, starch 3 g/L, $\text{MgSO}_4 \cdot 7\text{H}_2\text{O}$ 0.1 g/L, KH_2PO_4 1.5 g/L, Na_2HPO_4 2 g/L. The medium was adjusted to a pH of 7.8 and sterilised at 121°C for 20 min. The soil suspensions were pretreated at 80°C to kill non-*Bacillus* cells and then were mixed with MNPs following the determined mixture ratio. After shaking (150 rpm) for 20 min, the MNP-

functionalized part (cells and particles) was then separated from the aqueous phase using a permanent magnet, followed by resuspension in deionised water. This step was repeated three times to remove those bacteria that were not functionalized by MNPs. Subsequently, the MNP-functionalized parts were resuspended in 10 ml *Bacillus* enrichment medium and placed in an incubator at 37°C for 1 day.

After one-day incubation, a permanent magnet was used to separate non-MNP-functionalized cells (namely active *Bacillus*) from MNP-functionalized cells (namely inactive cells) and soil particles. The active Bacilli were split into two parts, one for DNA extraction and the other for cell imaging. *Bacillus* cellular suspension (1.5 μL) was loaded in the mini-wells of the chip and then was air-dried. Then we used a single-cell precision sorter (PRECI SCS; Hooke Instruments) equipped with SCIR to capture cell images of *Bacillus*. ImageJ was used to automatically count the size of *Bacillus* cells in the images, and Excel was used to calculate the frequency distribution of cell size within each fertilisation treatment.

2.3 | Molecular biology technology and statistical analyses

2.3.1 | DNA extraction

Bacillus DNA was extracted using the Bacterial genomic DNA extraction kit (TIANGEN, Beijing, China) according to the manufacturer's instructions. The extracted DNA was dissolved in 50 μL of TE buffer and was qualified by gel electrophoresis. After that, the extracted DNA was evaluated by NanoDrop 2000 (Thermo Fisher Scientific, US) for quantity and quality and stored at -20°C until further use.

2.4 | PCR and high-throughput amplicon sequencing

The genera-specific primer sets B-K1/F (5'-TCACCAAGGCRACGATGCG-3') and B-K1/R1 (5'-CGTATTCACCGCG GCATG -3') were used to amplify *Bacillus* 16S rRNA genes (Xu et al., 2018). Each PCR 50 μL reaction mixture contained 25 μL Taq DNA polymerase (TaKaRa, Japan), 2 μL gDNA (30–100 ng/ μL), 0.2 μL BSA (TaKaRa, Japan), 1 μL (10 Mm) of forward and reverse primers, 20.8 μL nuclease-free water. The negative control was always run with sterile water as the template instead of soil DNA extract. After initial denaturation at 94°C for 5 min, each thermal cycling was as follows: denaturation at 94°C for 30 s, annealing at 60°C for 40 s,

and elongation at 72°C for 1 min. At the end of 30 cycles, the final extension was performed at 72°C for 10 min. The PCR products were further sequenced with the primers 341F (5'-CCTACGGGNGGCWGCAG-3') and 805R (5'-GACTACHVGGGTATCTAATCC-3') targeting the V3–V4 hypervariable regions of bacterial 16S rRNA genes. The 12-bp bar-coded oligonucleotides were fused to the forward primer. Each PCR 50 µl reaction mixture contained 25 µl Q5 Ultra-fidelity DNA polymerase (NEB, America), 5 µl gDNA (30–100 ng/µL), 5 µl (10 µM) of forward and reverse primers, 10 µl nuclease-free water. Each sample was run with three replicates and the negative control was always run with sterile water as the template. The thermal cycling conditions were as follows: an initial denaturation at 95°C for 5 min, followed by 35 cycles at 95°C for 30 s, 55°C for 1 min, and 68°C for 2 min, with a final extension at 68°C for 10 min. PCR products for each sample were pooled and purified using the QIAquick PCR Purification Kit (Qiagen) and quantified using NanoDrop ND-2000 (Thermo Fisher Scientific, United States). High-throughput sequencing was performed with Illumina HiSeq sequencing platform (Illumina Inc.). The bar-coded PCR products from all samples were equimolarly normalised before sequencing. After sequencing, 16S rRNA genes data were processed using the Quantitative Insights into Microbial Ecology (QIIME, United States) pipeline for data sets. Sequences with a quality score below 20 and a length fewer than 200 bp were trimmed and then assigned to soil samples based on unique 5-bp barcodes. After denoising and chimera filtering using Usearch pipeline (Haas et al., 2011; Reeder & Knight, 2010), the quality reads were then binned into operational taxonomic units (OTUs) using a 97% identity threshold, and the most abundant sequence from each OTU was selected as the representative sequence. Taxonomy was then assigned to bacterial OTUs with reference to a subset of the RDP classifier. Raw sequencing data were uploaded to NCBI Sequence Read Archive (SRA) database under accession number PRJNA770877.

We obtained a total of 1,918,106 reads of bacterial 16S rRNA gene fragments. For all OTU-based analyses, the original OTU table was rarified to a depth of 38,419 reads per sample to measure both diversity and species composition patterns.

2.5 | Statistical analyses

Principal Coordinates Analysis (PCoA), based on Bray-Curtis distance, was carried out to visualise the effect of fertilisation on the *Bacillus* community. In addition, a permutational multivariate analysis of variance

(PERMANOVA) test was performed to test the dissimilarity significance among treatments. The “vegan” package of R software was used for the above analyses. Statistical analysis was conducted with one-way ANOVA followed by post-hoc Tukey's honestly significant different (HSD) tests using the IBM Statistical Product and Service Solutions (SPSS) Statistics for Windows (Version 16.0). The data were expressed as the means ($n = 3$) with standard deviation (SD); different letters indicate significant differences between different treatments ($p < 0.05$).

3 | RESULTS

3.1 | Optimal separation efficiency

To achieve the effective magnetic wrapping of all microbial cells and soil particles of soil suspension, the inflection point was considered as the optimal condition. From the curve of soil magnetic functionalization efficiency (Figure 1a), the OF, MF and CK MNP-functionalized soil samples were prepared by mixing 10 ml soil suspension and 1.6, 1.2, and 1.2 g MNPs, respectively. As shown in Figure 1b, the soil suspension and MNPs were mixed in the optimal ratio. After the part wrapped by MNPs was adsorbed by the magnet, the remaining part is clear and transparent. This proves again the optimal ratio of MNPs to soil suspension obtained from the experiment.

3.2 | Use the MMI method to reduce the background value

Compared with the conventional centrifuge method (Figure 2a), there were almost no large impurities in the visual field after MMI treatment (Figure 2b). In addition, the number of bare single cells increased due to the enrichment of *Bacillus* after culture in the process of MMI treatment. The bacterial suspension after treatment was directly used for DNA extraction and subsequent sequencing analysis.

3.3 | Divergent *Bacillus* composition under different fertilisation regimes

We assigned taxonomy against the SILVA database. More than 71%, 74%, and 78% of the bacteria screened in CK, MF and OF fertilised soils were from *Bacillus*, respectively (Figure 3a). This result demonstrated that MMI is a powerful tool to recover live and functional cells in situ from a complex microbial community, such as soil.

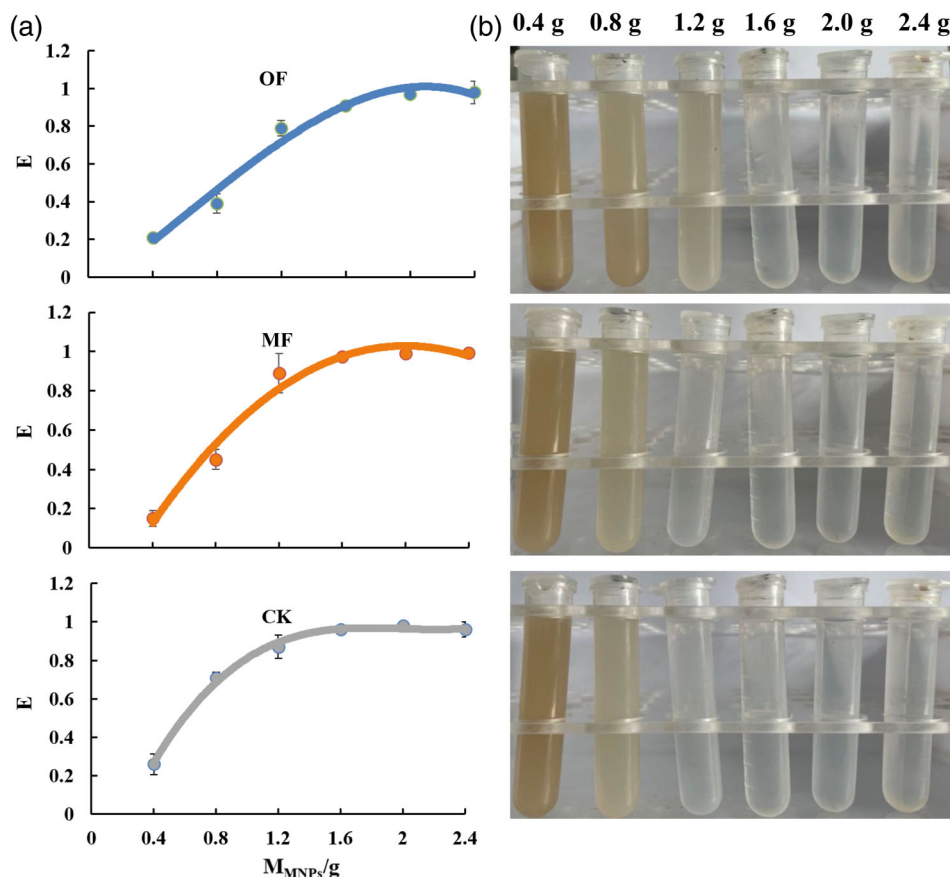


FIGURE 1 Optimal ratio of soil suspensions and magnetic MNPs. (a) Relationships between the magnetic functionalization efficiency of soil solution and the MNPs mass under three fertilisation regimes; (b) the remaining corresponding soil solution after removing the magnetic part. E: soil magnetic functionalization efficiency; CK, unfertilised control; MF, mineral fertilisation; OF, organic fertilisation

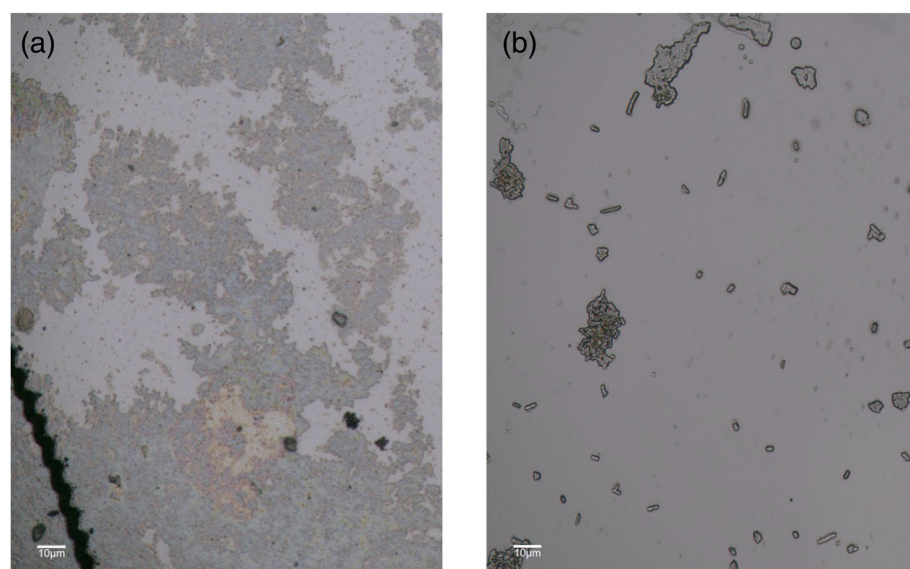


FIGURE 2 Use of the MMI method to reduce the background value. Soil suspensions (a) untreated and (b) treated with magnetic nanoparticle-mediated isolation

The NMDS plots (Figure 3b) and the result of the PERMANOVA test (Table 2) confirmed that there was no significant difference in the community structure of *Bacillus* under the three fertilisation regimes ($p > 0.05$).

The box-plot (Figure 4a) and frequency distribution figure (Figure 4b) of soil *Bacillus* size were made to assess the effects of different fertilisation regimes on the

Bacillus cell size. The data are shown in Figure 4a indicated that the *Bacillus* cell size presented a trend of OF > CK > MF, and there were significant differences ($p < 0.05$). For Figure 4b, the cell size has been divided into 6 intervals ($0-5 \mu\text{m}^2$, $5-10 \mu\text{m}^2$, $10-15 \mu\text{m}^2$, $15-20 \mu\text{m}^2$, $20-25 \mu\text{m}^2$ and $25-30 \mu\text{m}^2$), and the frequency of three fertilisation regions were statistically analysed in

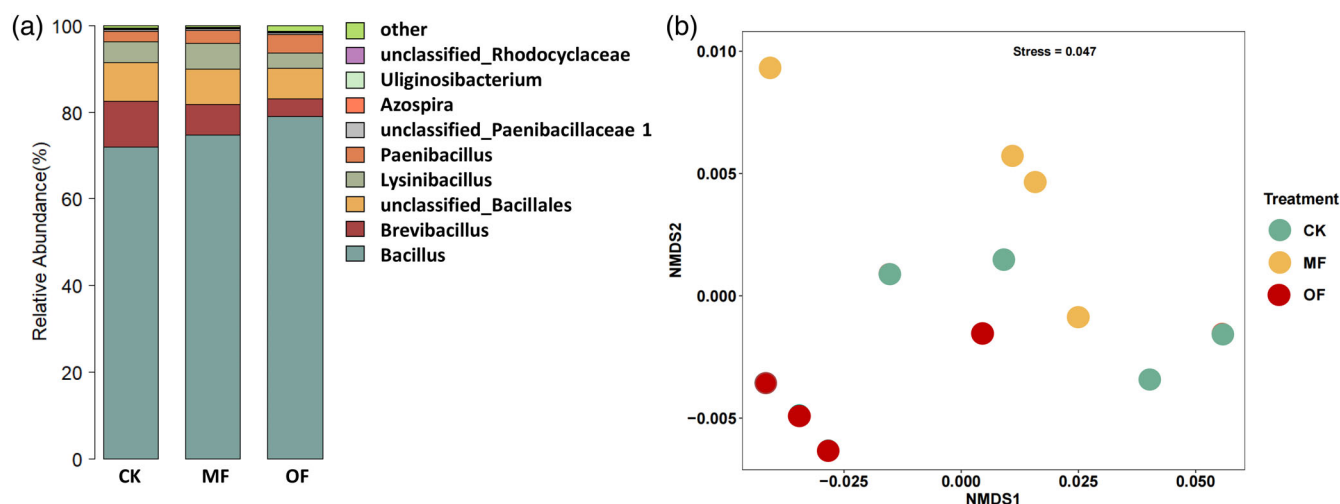


FIGURE 3 (a) Relative abundances and (b) nonmetric multidimensional scaling (NMDS) plot of *Bacillus* under three fertilisation regimes. CK, unfertilised control; MF, mineral fertilisation; OF, organic fertilisation

each interval. The cell size under OF and CK were mainly in the range of 5–10 μm^2 , while the cell size of MF was mainly in the range of 0–5 μm^2 . Only OF and CK treatments had cells in the range of 15–25 μm^2 , and the number of cells under OF treatment was more than that under CK. The only cells in the range of 25–30 μm^2 were found under OF treatment.

4 | DISCUSSION

Microbial morphology, which determines a wide range of life-history attributes, such as nutrient acquisition efficiency, is a key ecological characteristic of microorganisms (Bjorklund, 1866; Portillo et al., 2013). However, the response of cell size to soil environmental changes is still lacking. In this study, MMI combined with the SCIR method was employed to investigate the cell size of metabolically active soil *Bacillus* under three fertilizations.

4.1 | Visualising and isolating active *Bacillus* using coupled MMI and SCIR methods

The soil particles and soil organic matter are closely connected with biological organisms (Bronick & Lal, 2005), so it is difficult to separate the active functional microbes. As shown in Figure 2a (the soil suspension was treated with the conventional centrifuge method), no exposed single cell can be seen in the field of vision due to the dispersal of microbial cells in a large background of soil particles. This makes it difficult to observe the size of soil microorganisms in situ. The development of the MMI

method makes it possible. As shown in Figure 2b (the soil suspension was treated with the MMI method), we can clearly see the rod-shaped bacteria. To achieve this result, we firstly used hyperthermia inactivation to stop non-target organisms from growing and dividing. On this basis, one-day enrichment was used before magnetic separation in this study. Though one-day enrichment might slightly change the cell size and microbial community to a certain extent, it ensures that the active *Bacillus* grow and can be separated from soil and inactive microbes. In previous studies, the generally used molecular method could only investigate the whole genomic DNA in soils (Bahram et al., 2018; Delgado-Baquerizo et al., 2018). Here, the combination of MMI and SCIR approach in our study makes it possible to focus on the single-cell level. This improvement is beneficial for the integration of downstream analysis with microbial morphology (Chen et al., 2021; Gan et al., 2021). Therefore, the established experimental and analytical methods are based on MMI.

The abundance of microbes can reflect the ability to adjust themselves to changes in the soil environment. In this study, the amount of MNPs added to the OF treatment was higher than that of MF and CK treatments during the MMI approach (Figure 1a). This indicates that OF treatment harboured more microorganisms. High-throughput sequencing showed that a higher relative abundance of *Bacillus* was cultivated in OF treatment than in MF and CK treatments (Figure 3a). These results validate that OF fertilisation stimulates the abundance of *Bacillus*. The main reason is that long-term application of organic fertiliser increases the nutrient content in the soil, improves the soil structure, and makes the environmental conditions more suitable for the survival of soil *Bacillus* (such as increasing the porosity and the stability of soil

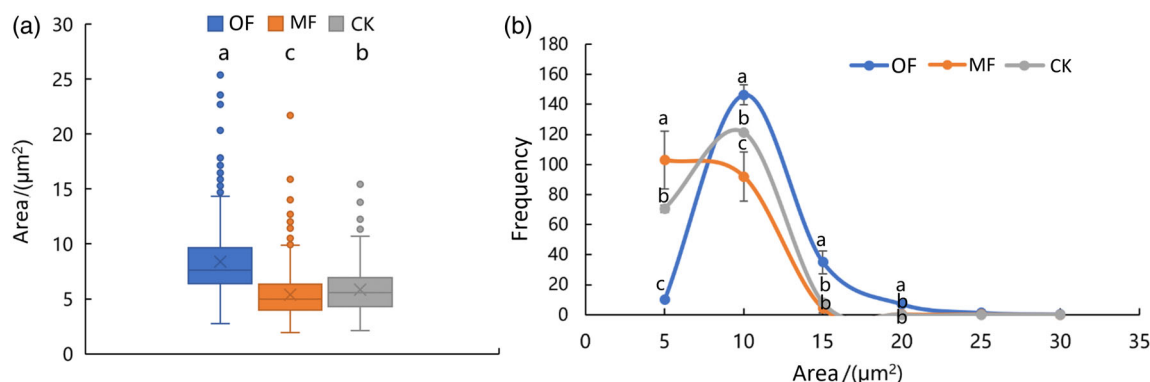


FIGURE 4 (a) Box-plot (a) and (b) the frequency distribution figure of soil *Bacillus* size under three fertilisation regimes. Different letters in the Figure represent the significant difference. CK, unfertilised control; MF, mineral fertilisation; OF, organic fertilisation

TABLE 2 Dissimilarity tests of metabolically active *Bacillus* communities between fertilisation treatments using permutational multivariate analysis

Pairs	F.Model	R ²	p
CK vs MF	0.86	0.13	0.46
CK vs OF	6.56	0.52	0.055
MF vs OF	2.69	0.31	0.12

Abbreviations: CK, unfertilised control; MF, mineral fertilisation; OF, organic fertilisation.

aggregates, etc.) (Bronick & Lal, 2005; Lin et al., 2019; Zhou et al., 2013). Thus, organic fertilisation increased the abundance of *Bacillus* by improving soil physicochemical properties. This result is consistent with our previous study, which demonstrated that organic fertilisation enlarges the abundance of *Bacillus* in the long-term fertilisation experiment of more than 30 years (Feng et al., 2015).

In this study, we demonstrated that a combination of MMI and SCIR can be used to observe the morphology of live functional cells from a complex environment, such as soil, and that cells can be used for further eco-physiological studies. This method can also be used to observe the morphology of functional microorganisms in other complex environments, for example by replacing carbon sources with pollutants.

4.2 | Stimulation of active *Bacillus* cell size under organic fertilisation

The size of microbes can reflect the ability to utilise the resources from the survival environment. Sargent et al. found that the length of *Bacillus subtilis* cells grown in a eutrophic medium was twice that of cells grown in an

oligotrophic medium (Sargent, 1975). Our study revealed that OF fertilisation significantly increased *Bacillus* cell size, using the SCIR results (Figure 4a). There may be two reasons for this result. First, different fertilisation regimes did not change the community structure of *Bacillus*, but only changed cell size. Secondly, different fertilisation regimes changed the community structure of *Bacillus* and then screened *Bacillus* of different sizes. As the fertilisation treatments did not change the community composition of active *Bacillus* according to the sequencing results (Table 2), it could be inferred that the former was the cause. We propose that the conditions in the OF treatment affected the cell size of *Bacillus*.

Firstly, the stimulation of *Bacillus* could be attributed to the change of soil pH in the OF treatment. The decreased soil pH in OF made the soil environment more conducive to the *Bacillus* community since the tested soil was alkaline, but the optimum pH for *Bacillus* growth is neutral (Xie et al., 2010).

Secondly, the increased nutrient availability in OF treatment was also beneficial for the growth of soil *Bacillus*. The nutrients in organic fertiliser need to be transformed into available forms by microorganisms before they can be absorbed. For single-celled organisms, cell size is the most powerful description of individual metabolic rate (Brown et al., 2016). Kempes et al. proposed that the total volume of a cell is the sum of the volumes of the ribosome, DNA and other substances (Kempes et al., 2016). Ribosomes, as a kind of organelle that helps protein synthesis, are closely related to biological metabolism (Noller, 2017; Steitz & Moore, 2017). Larger cells have higher metabolic activity due to their more numerous ribosomes (Kempes et al., 2016). The bigger size of *Bacillus* enhances the metabolic ability to decompose exogenous nutrients in the OF treatment soils.

In addition, UDP-glucose served as the intracellular proxy for nutrient availability and is thus at a higher

concentration in cells under organic fertilisation conditions. High intracellular concentrations of UDP-glucose stimulate glucosyltransferase localization to mid-cell where it interacts directly with the protein FtsZ to inhibit assembly and/or maturation of the FtsZ ring, increasing cell size (Chien et al., 2012; Kempes et al., 2012; Weart et al., 2007). In all, the increased cell sizes for all *Bacillus* phylotypes in the OF treatment compared to that of MF and CK could be attributed to the changed pH, the increased nutrient availability, and potential intracellular proxy in OF treatment.

5 | CONCLUSION

Our study demonstrated that the combination of MMI and SCIR methods can be used to identify the size and community composition of soil active *Bacillus*. In this investigation, we analysed *Bacillus* in soil samples from three contrasting long-term experimental fertilisation trials (mineral, organic or no fertilisation) using this approach, and showed that organic fertilisation stimulates the abundance and size of active *Bacillus* in soil. These results provide useful information for a better understanding of long-term different fertilisation effects on active microbes in alkaline soils. This work suggested that coupling MMI and SCIR can extend and improve the morphological investigation of microbes from complex environments at the single-cell level.

ACKNOWLEDGEMENTS

This work was supported by the National Natural Science Foundation of China (Project No. 41771294, 42177297), the Natural Science Foundation of Beijing, China (Grant No. 8182058), and Guangxi Key Science and Technology Innovation Base on Karst Dynamics (No. KDL&Guangxi 202008).

AUTHOR CONTRIBUTIONS

Nan Rong: Conceptualization (lead); data curation (lead); formal analysis (lead); investigation (lead); methodology (lead); visualization (lead); writing – original draft (lead); writing – review and editing (equal). **Shiying He:** Methodology (equal); resources (lead); supervision (supporting). **Bei Li:** Methodology (equal); resources (equal); software (equal). **Xiangui Lin:** Funding acquisition (lead); supervision (supporting). **Xiaoling Liu:** Funding acquisition (equal); resources (supporting). **Yongjie Yu:** Conceptualization (equal); formal analysis (equal); Funding acquisition (equal); supervision (equal); writing – original draft (equal); writing – review and editing (lead). **Youzhi Feng:** Conceptualization (equal); data curation (equal); investigation (equal); methodology

(equal); resources (supporting); supervision (lead); writing – review and editing (supporting).

CONFLICT OF INTERESTS

The authors declare that they have no known competing financial interests or personal relationships that could have appeared to influence the work reported in this paper.

DATA AVAILABILITY STATEMENT

The sequences were deposited in the NCBI SRA database (PRJNA770877).

ORCID

Yongjie Yu  <https://orcid.org/0000-0002-6454-8986>

Youzhi Feng  <https://orcid.org/0000-0002-8519-841X>

REFERENCES

- Bahram, M., Hildebrand, F., Forslund, S. K., Anderson, J. L., Soudzilovskaia, N. A., Bodegom, P. M., Bengtsson-Palme, J., Anslan, S., Coelho, L. P., Harend, H., Huerta-Cepas, J., Medema, M. H., Maltz, M. R., Munda, S., Olsson, P. A., Pent, M., Pölme, S., Sunagawa, S., Ryberg, M., ... Bork, P. (2018). Structure and function of the global topsoil microbiome. *Nature*, 560, 233. <https://doi.org/10.1038/s41586-018-0386-6>
- Berdugo, M., Delgado-Baquerizo, M., Soliveres, S., Hernández-Clemente, R., Zhao, Y., Gaitán, J. J., Gross, N., Saiz, H., Maire, V., Lehmann, A., Rillig, M. C., Solé, R. V., & Maestre, F. T. (2020). Global ecosystem thresholds driven by aridity. *Science*, 367, 787. <https://doi.org/10.1126/science.aay5958>
- Bjorklund, M. (1866). Cell size homeostasis: Metabolic control of growth and cell division. *Biochimica et Biophysica Acta-Molecular Cell Research*, 409-417, 2019–2417. <https://doi.org/10.1016/j.bbamcr.2018.10.002>
- Bronick, C. J., & Lal, R. (2005). Soil structure and management: a review. *Geoderma*, 124, 3–22. <https://doi.org/10.1016/j.geoderma.2004.03.005>
- Brown, C. T., Olm, M. R., Thomas, B. C., & Banfield, J. F. (2016). Measurement of bacterial replication rates in microbial communities. *Nature Biotechnology*, 34, 1256–1263. <https://doi.org/10.1038/nbt.3704>
- Chen, K., Liu, Z., Wang, X., Yu, C., Ye, J., Yu, C., Wang, F., & Shen, C. (2021). Enhancement of perchloroethene dechlorination by a mixed dechlorinating culture via magnetic nanoparticle-mediated isolation method. *Science of the Total Environment*, 786, 147421. <https://doi.org/10.1016/j.scitotenv.2021.147421>
- Chen, Y., Zhao, G., Zahumensky, J., Honey, S., & Fletcher, B. (2020). Differential scaling of gene expression with cell size may explain size control in budding yeast. *Molecular Cell*, 78, 359–+. <https://doi.org/10.1016/j.molcel.2020.03.012>
- Chien, A.-C., Hill, N. S., & Levin, P. A. (2012). Cell size control in bacteria. *Current Biology*, 22, R340–R349. <https://doi.org/10.1016/j.cub.2012.02.032>
- Delgado-Baquerizo, M., Oliverio, A. M., Brewer, T. E., Benavent-González, A., Eldridge, D. J., Bardgett, R. D., Maestre, F. T., Singh, B. K., & Fierer, N. (2018). A global atlas of the dominant

- bacteria found in soil. *Science*, 359, 320–+. <https://doi.org/10.1126/science.aap9516>
- Eichorst, S. A., Strasser, F., Woyke, T., Schintlmeister, A., Wagner, M., & Wobken, D. (2015). Advancements in the application of NanoSIMS and Raman microspectroscopy to investigate the activity of microbial cells in soils. *FEMS Microbiology Ecology*, 91, fiv106. <https://doi.org/10.1093/femsec/fiv106>
- Feng, Y., Chen, R., Hu, J., Zhao, F., Wang, J., Chu, H., Zhang, J., Dolfing, J., & Lin, X. (2015). *Bacillus asahii* comes to the fore in organic manure fertilized alkaline soils. *Soil Biology and Biochemistry*, 81, 186–194. <https://doi.org/10.1016/j.soilbio.2014.11.021>
- Gan, C., Wu, R., Luo, Y., Song, J., Luo, D., Li, B., Yang, Y., & Xu, M. (2021). Visualizing and isolating iron-reducing microorganisms at the single-cell level. *Applied and Environmental Microbiology*, 87, e02192–20. <https://doi.org/10.1128/aem.02192-20>
- Ginzberg, M. B., Kafri, R., & Kirschner, M. (2015). On being the right (cell) size. *Science*, 348, 1245075. <https://doi.org/10.1126/science.1245075>
- Haas, B. J., Gevers, D., Earl, A. M., Feldgarden, M., Ward, D. V., Giannoukos, G., Ciulla, D., Tabbaa, D., Highlander, S. K., Sodergren, E., Methé, B., DeSantis, T. Z., The Human Microbiome Consortium, Petrosino, J. F., Knight, R., & Birren, B. W. (2011). Chimeric 16S rRNA sequence formation and detection in sanger and 454-pyrosequenced PCR amplicons. *Genome Research*, 21, 494–504. <https://doi.org/10.1101/gr.112730.110>
- Healy, K., McNally, L., Ruxton, G. D., Cooper, N., & Jackson, A. L. (2013). Metabolic rate and body size are linked with perception of temporal information. *Animal Behaviour*, 86, 685–696. <https://doi.org/10.1016/j.anbehav.2013.06.018>
- Hill, N. S., Kadota, R., Chatteraj, D. K., & Levin, P. A. (2012). Cell size and the initiation of DNA replication in bacteria. *PLoS Genetics*, 8, e1002549. <https://doi.org/10.1371/journal.pgen.1002549>
- Kempes, C. P., Dutkiewicz, S., & Follows, M. J. (2012). Growth, metabolic partitioning, and the size of microorganisms. *Proceedings of the National Academy of Sciences of the United States of America*, 109, 495–500. <https://doi.org/10.1073/pnas.1115585109>
- Kempes, C. P., Wang, L., Amend, J. P., Doyle, J., & Hoehler, T. (2016). Evolutionary tradeoffs in cellular composition across diverse bacteria. *ISME Journal*, 10, 2145–2157. <https://doi.org/10.1038/ismej.2016.21>
- Li, J. B., Luo, C. L., Zhang, G., & Zhang, D. Y. (2018). Coupling magnetic-nanoparticle mediated isolation (MMI) and stable isotope probing (SIP) for identifying and isolating the active microbes involved in phenanthrene degradation in wastewater with higher resolution and accuracy. *Water Research*, 144, 226–234. <https://doi.org/10.1016/j.watres.2018.07.036>
- Lin, Y., Ye, G., Kuzyakov, Y., Liu, D., Fan, J., & Ding, W. (2019). Long-term manure application increases soil organic matter and aggregation, and alters microbial community structure and keystone taxa. *Soil Biology and Biochemistry*, 134, 187–196. <https://doi.org/10.1016/j.soilbio.2019.03.030>
- Lloyd, A. C. (2013). The regulation of cell size. *Cell*, 154, 1194–1205. <https://doi.org/10.1016/j.cell.2013.08.053>
- Lobell, D. B., & Field, C. B. (2007). Global scale climate - crop yield relationships and the impacts of recent warming. *Environmental Research Letters*, 2, 014002. <https://doi.org/10.1088/1748-9326/2/1/014002>
- Lu, A. H., Salabas, E. L., & Schuth, F. (2007). Magnetic nanoparticles: Synthesis, protection, functionalization, and application. *Angewandte Chemie-International Edition*, 46, 1222–1244. <https://doi.org/10.1002/anie.200602866>
- Miettinen, T. P., & Bjorklund, M. (2016). Cellular allometry of mitochondrial functionality establishes the optimal cell size. *Developmental Cell*, 39, 370–382. <https://doi.org/10.1016/j.devcel.2016.09.004>
- Miettinen, T. P., & Bjorklund, M. (2017). Mitochondrial function and cell size: An Allometric relationship. *Trends in Cell Biology*, 27, 393–402. <https://doi.org/10.1016/j.tcb.2017.02.006>
- Nicholson, W. L., Munakata, N., Horneck, G., Melosh, H. J., & Setlow, P. (2000). Resistance of *Bacillus* endospores to extreme terrestrial and extraterrestrial environments. *Microbiology and Molecular Biology Reviews*, 64, 548–572. <https://doi.org/10.1128/mmbr.64.3.548-572.2000>
- Noller, H. F. (2017). The parable of the caveman and the Ferrari: Protein synthesis and the RNA world. *Philosophical Transactions of the Royal Society B-Biological Sciences*, 372, 20160187. <https://doi.org/10.1098/rstb.2016.0187>
- Pohl, S., & Harwood, C. R. (2010). Heterologous protein secretion by *Bacillus* species: From the cradle to the grave. *Advances in Applied Microbiology*, 73, 1–25. [https://doi.org/10.1016/S0065-2164\(10\)73001-X](https://doi.org/10.1016/S0065-2164(10)73001-X)
- Portillo, M. C., Leff, J. W., Lauber, C. L., & Fierer, N. (2013). Cell size distributions of soil bacterial and archaeal taxa. *Applied and Environmental Microbiology*, 79, 7610–7617. <https://doi.org/10.1128/aem.02710-13>
- Reeder, J., & Knight, R. (2010). Rapidly denoising pyrosequencing amplicon reads by exploiting rank-abundance distributions. *Nature Methods*, 7, 668–669. <https://doi.org/10.1038/nmeth0910-668b>
- Sargent, M. G. (1975). Control of cell length in *Bacillus-subtilis*. *Journal of Bacteriology*, 123, 7–19. <https://doi.org/10.1128/jb.123.1.7-19.1975>
- Slessarev, E. W., Lin, Y., Bingham, N. L., Johnson, J. E., Dai, Y., Schimel, J. P., & Chadwick, O. A. (2016). Water balance creates a threshold in soil pH at the global scale. *Nature*, 540, 567. <https://doi.org/10.1038/nature20139>
- Steitz, T. A., & Moore, P. B. (2017). Perspectives on the ribosome. *Philosophical Transactions of the Royal Society B: Biological Sciences*, 372, 20160537. <https://doi.org/10.1098/rstb.2016.0537>
- Takahashi, M., Nakanishi, H., Kawasaki, S., Nishizawa, N. K., & Mori, S. (2001). Enhanced tolerance of rice to low iron availability in alkaline soils using barley nicotianamine aminotransferase genes. *Nature Biotechnology*, 19, 466–469. <https://doi.org/10.1038/88143>
- Ursell, T., Lee, T. K., Shiomi, D., Shi, H., Tropini, C., Monds, R. D., Colavin, A., Billings, G., Bhaya-Grossman, I., Broxton, M., Huang, B. E., Niki, H., & Huang, K. C. (2017). Rapid, precise quantification of bacterial cellular dimensions across a genomic-scale knockout library. *BMC Biology*, 15, 17. <https://doi.org/10.1186/s12915-017-0348-8>

- Wang, X. Z., Zhao, X., Li, H., Jia, J., Liu, Y., Ejenavi, O., Ding, A., Sun, Y., & Zhang, D. (2016). Separating and characterizing functional alkane degraders from crude-oil-contaminated sites via magnetic nanoparticle-mediated isolation. *Research in Microbiology*, 167, 731–744. <https://doi.org/10.1016/j.resmic.2016.07.004>
- Weart, R. B., Lee, A. H., Chien, A. C., Haeusser, D. P., Hill, N. S., & Levin, P. A. (2007). A metabolic sensor governing cell size in bacteria. *Cell*, 130, 335–347. <https://doi.org/10.1016/j.cell.2007.05.043>
- Xie, Y., Xu, J.-H., & Xu, Y. (2010). Isolation of a *Bacillus* strain producing ketone reductase with high substrate tolerance. *Bioresource Technology*, 101, 1054–1059. <https://doi.org/10.1016/j.biortech.2009.09.003>
- Xu, Z., Cao, L., Liu, J., Tan, H., & Deng, Z. (2018). Evaluation of the diversity of probiotic *Bacillus*, *Clostridium*, and *Bifidobacterium* using the Illumina-based sequencing method. *Probiotics and Antimicrobial Proteins*, 10, 748–754. <https://doi.org/10.1007/s12602-017-9337-z>
- Young, K. D. (2006). The selective value of bacterial shape. *Microbiology and Molecular Biology Reviews*, 70, 660. <https://doi.org/10.1128/mmbr.00001-06>
- Zhang, D. Y., Berry, J. P., Zhu, D., Wang, Y., Chen, Y., Jiang, B., Huang, S., Langford, H., Li, G., Davison, P. A., Xu, J., Aries, E., & Hunag, W. E. (2015). Magnetic nanoparticle-mediated isolation of functional bacteria in a complex microbial community. *ISME Journal*, 9, 603–614. <https://doi.org/10.1038/ismej.2014.161>
- Zhou, H., Peng, X., Perfect, E., Xiao, T., & Peng, G. (2013). Effects of organic and inorganic fertilization on soil aggregation in an Ultisol as characterized by synchrotron based X-ray micro-computed tomography. *Geoderma*, 195–196, 23–30. <https://doi.org/10.1016/j.geoderma.2012.11.003>

How to cite this article: Rong, N., He, S., Li, B., Lin, X., Liu, X., Yu, Y., & Feng, Y. (2022). Coupled magnetic nanoparticle-mediated isolation and single-cell image recognition to detect *Bacillus* cell size in soil. *European Journal of Soil Science*, 73(3), e13236. <https://doi.org/10.1111/ejss.13236>